MADPH-00-1181
FERMILAB-Pub-00/113-T
hep-ph/0005306
May, 2000

Fermilab

Top-quark couplings to TeV resonances at future lepton colliders

T. Han[a], Y.J. Kim[a], A. Likhoded[b], and G. Valencia[c,d]

[a]Department of Physics, University of Wisconsin, Madison, WI 53706

[b]Institute for High Energy Physics, Protvino, Russia

[c]Department of Physics and Astronomy, Iowa State University, Ames, IA 50011

[d]Fermi National Accelerator Laboratory, Batavia, IL 60510

FERMILAB-Pub-00/113-T June 2000

Abstract

We study the processes $W_L W_L \to t\bar{t}$ and $W_L Z_L \to t\bar{b}$ ($\bar{t}b$) at future lepton colliders as probes of the couplings of the top quark to resonances at the TeV scale. We consider the cases in which the dominant low energy feature of a strongly interacting electroweak symmetry breaking sector is either a scalar or a vector resonance with mass near 1 TeV. We find that future lepton colliders with high energy and high luminosity have great potential to sensitively probe these physics scenarios. In particular, at a 1.5 TeV linear collider with an integrated luminosity of 200 fb^{-1}, we expect about 120 events for either a scalar or a vector to decay to $t\bar{t}$, tb. Their leading partial decay widths, which characterize the coupling strengths, can be statistically determined to about 10% level.

1 Introduction

The mass generation mechanisms for electroweak gauge bosons and for fermions are among the most prominent mysteries in contemporary high energy physics. In the standard model (SM) and its supersymmetric extensions, elementary scalar doublets of the $\mathrm{SU}(2)_L$ interactions are responsible for the mass generation. Yet there is no explanation for the scalar-fermion Yukawa couplings. On the other hand, if there is no light Higgs boson found in the next generation of collider experiments, then the interactions among the longitudinal vector bosons would become strong at a scale of $\mathcal{O}(1\ \mathrm{TeV})$ and new dynamics must set in [1]. The fact that the top-quark mass is very close to the electroweak scale ($m_t \approx v/\sqrt{2}$) is rather suggestive: there may be a common origin for electroweak symmetry breaking and top-quark mass generation. Much theoretical work has been carried out recently in connection to the top quark and the electroweak sector [2, 3, 4].

Due to the Goldstone boson equivalence theorem (ET) [5], the longitudinal gauge bosons ($W_L^{\pm}, Z_L$) resemble the Goldstone modes ($w^{\pm}, z$) at energies much larger than their mass M_W and thus faithfully reflect the nature of the electroweak symmetry breaking (EWSB). To study the EWSB sector in connection with the top quark, a sensitive probe is to produce a top quark via longitudinal gauge boson scattering [6]

$$W_L^+ W_L^-,\ Z_L Z_L \to t\bar{t}, \tag{1}$$

$$W_L^{\pm} Z_L \to t\bar{b}, \bar{t}b. \tag{2}$$

These processes will receive significant enhancement if there are underlying resonances in this sector that couple to both Goldstone bosons and the top quark. In particular, it is interesting to note that both a scalar (Higgs-like) resonance and a vector (techni-rho-like ρ^0) resonance would contribute to $W_L^+ W_L^- \to t\bar{t}$ in process (1); while only a vector (techni-rho-like $\rho^{\pm}$)

resonance would significantly enhance process (2).

These processes can be effectively realized at high energy lepton colliders via nearly collinear gauge boson radiation

$$e^+e^- \to \nu\bar{\nu}\ W_L^* W_L^* \to \nu\bar{\nu}\ t\bar{t}, \tag{3}$$

$$e^+e^- \to e\nu\ W_L^* Z_L^* \to e\nu\ tb, \tag{4}$$

where $e\nu\ tb$ generically denotes $e^-\bar{\nu}\ t\bar{b}$ and $e^+\nu\ \bar{t}b$. Within the effective W-boson approximation (EWA) [7], the $t\bar{t}$ production of Eq. (1) was first calculated in Ref. [8] and then in Ref. [9]. In the approach of an electroweak effective Lagrangian, they were studied in Ref. [10]. A full evaluation of the SM diagrams was performed for $t\bar{t}$ production at a 1.5 TeV linear collider [11, 12] and at a multi-TeV muon collider [13]. Effects on $W_L^+W_L^- \to t\bar{t}$ from other strongly interacting dynamics were recently discussed in [14, 15].

In this paper, we carry out a comprehensive evaluation for processes (3) and (4) within and beyond the SM. In Sec. 2, we first formulate the effective interactions for a strongly-interacting electroweak sector (SEWS) including the heavy top quark (Top-SEWS). We parameterize the sector in a (relatively) model-independent way by introducing a heavy scalar or a heavy vector to unitarize (up to a few TeV) the universal low-energy amplitudes [16]. We also comment on the current low-energy constraints on this sector. In Sec. 3, we perform detailed numerical analyses for the Top-SEWS signal and the SM backgrounds. We present our results at an e^+e^- linear collider with a center-of-mass energy $\sqrt{s} = 1.5$ and also illustrate some results at a lepton collider with CM energy of 4 TeV. We find that the future high energy lepton colliders have substantial potential to explore the Top-SEWS sector to great precision. Section 4 contains our conclusions. Some useful formulae are presented in Appendix A.

2 Effective Interactions in the Top-SEWS Sector

2.1 Low Energy Amplitudes

The low energy behavior of the scattering amplitudes for the processes $V_L V_L \to q\bar{q}$ is determined by symmetry, and is the same in all models in which the electroweak symmetry is broken by a strong interaction. If we parameterize the scale of this strong interaction with the mass of its lightest resonance M_R, then in the region where $m_W \ll \sqrt{s} \ll M_R$, the amplitudes are dominated by the low energy theorems (LET). These low energy theorems can be obtained in a simple manner with the use of the Goldstone-boson equivalence theorem as in Refs. [5, 6].

The framework for a model-independent analysis is that of effective Lagrangians. Within this framework, the low energy amplitudes arise from the lowest dimension operator one can construct that respects the symmetries of the standard model. The non-renormalizable effective Lagrangian responsible for the low energy interactions of the would-be Goldstone bosons $w^{\pm}, z$ is given by

$$\mathcal{L} = \frac{v^2}{4}\mathrm{Tr}\Big(\partial_\mu U^\dagger \partial^\mu U\Big) \tag{5}$$

where $U = \exp(iw^i\tau_i/v)$ [16, 17], with $\mathrm{Tr}\tau_i\tau_j = 2\delta_{ij}$ and $v \approx 246$ GeV. The minimal interactions between third generation fermions and the would-be Goldstone bosons are those of the standard model in the limit $M_H \to \infty$ and can be found, for example, in Refs. [6, 18]. We work in the limit $m_b = 0$ and find (for terms with up to two $w^{\pm}, z$),

$$\mathcal{L} = -i\frac{m_t}{v}\; z\;\overline{t}\gamma_5 t + \frac{im_t}{\sqrt{2}v}\;\Big(w^+\overline{t}(1-\gamma_5)b - w^-\overline{b}(1+\gamma_5)t\Big) + \frac{m_t}{v^2}\;\overline{t}t\Big(w^+w^- + \frac{1}{2}zz\Big). \tag{6}$$

As a benchmark we will consider the low energy amplitudes (LET) defined as the

dominant terms in the limits $M_W \ll (\sqrt{s},\ m_t) \ll (M_R,\ 4\pi v)$. Taking the scattering angle θ to be that between the momentum of the w^- (or z) and the top quark in the center of mass frame, we find for the neutral channels,

$$\begin{aligned}
\mathcal{M}^{++}{}_{LET}(ww \to t\bar{t}) &= -\mathcal{M}^{--}{}_{LET}(ww \to t\bar{t}) = -\frac{m_t\sqrt{s}}{v^2}\beta_t \qquad (7)\\
\mathcal{M}^{\pm\mp}{}_{LET}(ww \to t\bar{t}) &= \frac{m_t^2}{v^2}\frac{(1\pm\beta_t)\sin\theta}{1+\beta_t\cos\theta - 2m_t^2/s}\\
\mathcal{M}^{++}{}_{LET}(zz \to t\bar{t}) &= -\mathcal{M}^{--}{}_{LET}(zz \to t\bar{t}) = -\frac{m_t\sqrt{s}}{v^2}\beta_t\\
\mathcal{M}^{\pm\mp}{}_{LET}(zz \to t\bar{t}) &= -\frac{m_t^2}{v^2}\frac{\sin\theta}{1+\beta_t\cos\theta},
\end{aligned}$$

where $\beta_t = (1-4m_t^2/s)^{1/2}$.

For the charged $wz \to t\bar{b}$ channel we define the angle θ between the momentum of the z and the top quark in the center of mass frame, to obtain

$$\begin{aligned}
\mathcal{M}^{++}{}_{LET}(w^+z \to t\bar{b}) &= \frac{\sqrt{2}m_t^3}{v^2\sqrt{s}}\frac{\beta_m(1+\cos\theta)}{[\beta_m^2(1-\cos\theta)+2m_t^2/s]}\\
\mathcal{M}^{-+}{}_{LET}(w^+z \to t\bar{b}) &= -\frac{\sqrt{2}m_t^2}{v^2}\frac{\beta_m\sin\theta}{[\beta_m^2(1-\cos\theta)+2m_t^2/s]}. \qquad (8)
\end{aligned}$$

In writing these equations we took $M_W = m_b = 0$, and $\beta_m = (1-m_t^2/s)^{1/2}$. We present some details in Appendix A.

The low energy amplitude for the process $ww \to t\bar{t}$ in Eq. (7) grows linearly with energy and violates partial wave unitarity at an energy $\sqrt{s_{ww}} \approx 3$ TeV [19, 20]. Similarly, the low energy amplitude for the process $ww \to ww$ violates unitarity around 1.2 TeV [17, 21]. The energy scale at which these violations of unitarity take place can be interpreted as the

scale at which new physics must come into play. For our present purpose, the new physics that restores unitarity will be either a scalar or a vector resonance and we discuss these two cases in the next two sections. To maintain a model-independent discussion, we introduce the resonances through effective (non-renormalizable) low energy Lagrangians. Therefore, after inclusion of the resonance, the partial wave amplitudes will still violate unitarity at higher energies. We will adjust the couplings of the resonances so that violation of unitarity does not occur until a scale between 2 and 5 TeV. With this prescription, we describe the phenomenology of a resonance which is the dominant dynamical feature of a strongly interacting electroweak symmetry breaking sector (SEWS) below 2 TeV.

2.2 Scalar Resonance

The interactions between the standard model gauge bosons and a generic scalar resonance S, have been considered in Ref. [22]. The leading order effective Lagrangian for these interactions contains two free parameters: the resonance mass M_S and a coupling constant g_S that can be traded for the width of the new resonance into W and Z pairs. The effective Lagrangian for the scalar resonance and its interactions with the $w^{\pm}, z$ is given by

$$\mathcal{L} = \frac{1}{2}\partial_\mu S \partial^\mu S - \frac{1}{2}M_S^2 S^2 + \frac{1}{2}g_s v S \mathrm{Tr}\Big(\partial_\mu U^\dagger \partial^\mu U\Big) \tag{9}$$

from which one obtains that,

$$\Gamma_{Sww} = \frac{3}{32\pi}\frac{g_S^2 M_S^3}{v^2}. \tag{10}$$

With $g_S = 1$, Eq. (10) reproduces the width of the standard model Higgs boson.

It is straightforward to compute the amplitudes for $ww \to ww$ scattering in this

model. They are obtained from the Lagrangians, Eqs. (5) and (9). For example we find,

$$A(w^+w^- \to zz) = \frac{s}{v^2}\frac{s(1-g_S^2) - M_S^2}{s - M_S^2}. \tag{11}$$

All the other channels can be obtained from this one by using custodial $SU(2)$ and crossing symmetries [17]. From Eq. (11), we can see that the choice $g_S = 1$ reproduces the standard model amplitude. In this case, the amplitude takes a constant value at high energies as corresponds to the renormalizable standard model. If $g_S \neq 1$, however, the amplitude grows with energy violating unitarity at some point. To study this issue, we construct the $I = 0, J = 0$ partial wave amplitude,

$$\begin{aligned} a_0^0(s) &= -\frac{\Gamma_{Sww}}{g_S^2 M_S}\frac{s}{s - M_S^2 + i\Gamma_{Sww}\frac{s}{M_S}}\left(1 + \frac{s}{M_S^2}(g_S^2 - 1)\right) \\ &+ \frac{\Gamma_{Sww}}{3g_S^2 M_S}\left(\frac{s}{M_S^2}(g_S^2 - 1) - 2g_S^2\left[1 - \frac{M_S^2}{s}\log\left(1 + \frac{s}{M_S^2}\right)\right]\right). \end{aligned} \tag{12}$$

To obtain this result we have introduced a scalar-resonance width into the s-channel Higgs propagator according to the prescription of Ref. [23],

$$\frac{1}{s - M_S^2} \to \frac{1 + i\frac{\Gamma}{M_S}}{s - M_S^2 + i\Gamma\frac{s}{M_S}}. \tag{13}$$

which produces a well behaved amplitude both near the resonance and at high energy.*

We first look at this result in the region above the resonance, and near the limit of validity of the effective theory. For $\sqrt{s} \gg M_S$, Eq. (12) reduces to

$$a_0^0(s) = (1 - g_S^2)\frac{s}{16\pi v^2} - \frac{5}{3}\frac{\Gamma_{Sww}}{M_S} \tag{14}$$

*Both a constant width and an energy dependent width for a heavy scalar (with mass near 1 TeV) produce undesirable features [24]. We thank S. Willenbrock for pointing out reference [23].

Once again, we see that $g_S = 1$ reproduces the standard model result, in which the unitarity condition becomes a constraint on the Higgs boson mass [5]. The first term shows how, for $g_S \neq 1$, the model corresponds to a non-renormalizable effective theory. If we demand that this term satisfy a unitarity condition $|\mathrm{Re}(a_0^0(s))| < 0.5$ up to $\sqrt{s} = 2$ (3) TeV we obtain 0.8 $(0.9) \leq |g_S| \leq 1.2$ (1.1). If we choose to consider all the effects of the resonance, including its width according to the prescription of Ref. [23], we then find for $M_S = 1$ TeV that unitarity condition in the form $|a_0^0| < 1$, is satisfied up to 2 (5) TeV with

$$0.4\ (0.9) \leq |g_S| \leq 1.1\ (1.02). \tag{15}$$

The effective Lagrangian describing the coupling of the top quark to the scalar resonance that we use is,

$$\mathcal{L} = -\kappa \frac{m_t}{v} S \bar{t} t \tag{16}$$

where κ is a new coupling that can be traded for the width of the scalar into top-quark pairs,

$$\Gamma_{St\bar{t}} = \frac{3\kappa^2}{8\pi} \frac{m_t^2 M_S}{v^2} \left(1 - \frac{4m_t^2}{M_S^2}\right)^{\frac{3}{2}}. \tag{17}$$

The case $\kappa = 1$ corresponds to the usual standard model Higgs-boson coupling to the top quark. With Eqs. (5), (9) and (16), we have an effective theory involving a new generic scalar resonance and its couplings to would-be Goldstone bosons and top quarks. Using Eqs. (9) and (16), and the Equivalence Theorem (ET), we find the matrix element for $W_L W_L \to t\bar{t}$ via the scalar S to be

$$\mathcal{M}_S^{+\,+}(ww \to t\bar{t}) = -\mathcal{M}_S^{-\,-}(ww \to t\bar{t}) = g_S \kappa \frac{s}{s - M_S^2} \frac{m_t \sqrt{s}}{v^2} \beta_t, \tag{18}$$

here and henceforth, the double superscripts denote the $t\bar{t}$ helicities. For $\kappa = g_S = 1$, it reduces to the standard model result. We obtain identical amplitudes for $zz \to t\bar{t}$. To

describe the resonance region we modify this amplitude according to the prescription in Ref. [23]. Having chosen an $SU(2)$ singlet, electrically neutral, scalar resonance, there is no contribution to $W_L^{\pm}Z_L \to t\bar{b}, \bar{t}b$ in this model.

There are no significant, phenomenological constraints on the couplings g_S and κ. Following Refs. [6], [19], and [25], we can demand that the process $ww \to t\bar{t}$ satisfy inelastic partial-wave unitarity. By choosing the $I = 0, J = 0$, color singlet channel as in Ref. [20], we find,

$$\left|3\frac{G_F m_t\sqrt{s}}{8\pi\sqrt{2}}\right|\left|\frac{M_S^2 + s(g_S\kappa - 1)}{s - M_S^2}\right| < 0.5 \tag{19}$$

In analogy with our treatment of Eq. (12), we first concentrate in the region above the resonance. The first factor in Eq. (19) corresponds to the low energy theorem, and it violates unitarity at $\sqrt{s} \approx 3$ TeV. We can have the full amplitude satisfy unitarity up to 3 TeV by requiring the second factor to satisfy

$$\left|g_S\kappa\frac{s}{s - M_S^2} - 1\right| < 1 \tag{20}$$

or, for energies far above the resonance, $0 < g_S\kappa < 2$.

If, on the other hand, we introduce the width according to the prescription of Ref. [23] and consider the full amplitude for $M_S = 1$ TeV, unitarity is satisfied up to $\sqrt{s} = 2$ (5) TeV if

$$0\ (0.4) < g_s\kappa < 1.9\ (1.6) \tag{21}$$

Finally, we consider $t\bar{t} \to t\bar{t}$ scattering at energies above the resonance (in the same helicity, color singlet channel). The $J = 0$ partial wave is,

$$a_0(t\bar{t} \to t\bar{t}) = -\frac{3}{4\pi}\frac{G_F m_t^2}{\sqrt{2}}\kappa^2. \tag{22}$$

If we follow Ref. [20] and require that $|\mathrm{Re}a_0(t\bar{t} \to t\bar{t})| < 0.5$, we obtain the unitarity constraint

$$|\kappa| < 2.9. \tag{23}$$

As we will see in our numerical studies in Fig. 8, this constraint is not very restrictive.

2.3 Vector Resonance

The interactions of standard model gauge bosons with new vector resonances have been described in the literature [26, 27]. In the notation of Ref. [26], two new parameters are introduced a and $\tilde{g}$ (these correspond to α and $g''/2$ from Ref. [27], respectively). The effective Lagrangian consists of a kinetic term for the triplet of vector resonances $\rho_\mu \equiv \rho^i_\mu \tau_i/2$ and an interaction term of the form

$$\mathcal{L} = -\frac{1}{4} a v^2 \mathrm{Tr}\Big((\xi^\dagger \partial_\mu \xi + \xi \partial_\mu \xi^\dagger + i2\tilde{g}\rho_\mu)(\xi^\dagger \partial^\mu \xi + \xi \partial^\mu \xi^\dagger + i2\tilde{g}\rho^\mu) \Big) \tag{24}$$

where $\xi = \exp(iw^i \tau_i/2v)$.

The two new constants $a, \tilde{g}$ are related to the mass and width of the vector particles ρ via the relations,

$$M_\rho^2 = a v^2 \tilde{g}^2, \quad \Gamma(\rho^0 \to w^+ w^-) = \frac{a^2 \tilde{g}^2}{192\pi} M_\rho. \tag{25}$$

In addition, when the electroweak gauge bosons are added in a gauge invariant manner, they mix with the new vector bosons [27]. In the charged sector, the physical states become,

$$V^\pm_{ph} = \rho^\pm \cos\phi + W^\pm \sin\phi, \qquad W^\pm_{ph} = W^\pm \cos\phi - \rho^\pm \sin\phi \tag{26}$$

with a mixing angle given by

$$\tan 2\phi = \frac{4ag\tilde{g}}{(1+a)g^2 - 4a\tilde{g}^2} \to -\frac{g}{\tilde{g}}, \tag{27}$$

the last expression being the limit as $M_\rho \to \infty$. Similar expressions for the mixing in the neutral sector can be found in the literature [27]. For our numerical studies we use couplings a, $\tilde{g}$ that have been studied in detail by the authors of the BESS model, and that respect partial wave unitarity below a few TeV. For example, for $M_\rho = 1$ TeV and $\Gamma_\rho = 30$ GeV, the partial wave a_0^0 for $ww \to ww$ scattering satisfies $|a_0^0| < 1$ up to about 2.6 TeV, while $|a_1^1| < 1$ is satisfied up to about 3 TeV with the simple prescription of using a constant width in the s-channel ρ propagator.

We are currently interested in effective couplings between the new vector mesons and the top and bottom quarks. These couplings may arise either from the ordinary quark couplings to gauge bosons through the mixing of Eq. (26), or from novel direct couplings. The couplings induced by mixing are universal, common to the three generations, and can be bound by low energy experiments. More interesting is the possibility of a direct coupling to the third generation. We write these effective couplings in a generic form

$$\mathcal{L}_{eff} = -\bar{\psi}\gamma^\mu(g_V + g_A\gamma_5)\tau^i\psi\ \rho_\mu^i, \tag{28}$$

where $\bar{\psi}$ is the third generation quark doublet $(\bar{t}\ \bar{b})$.

Unlike the case of the scalar resonance, there exist low energy constraints on the direct couplings of new vector resonances to the third generation quarks because they modify their couplings to the W and Z. These deviations can be parameterized by the low energy effective Lagrangian

$$\begin{aligned}\mathcal{L}_{eff} &= -\frac{g}{\sqrt{2}}\Big[(1+\delta\kappa_L)\bar{t}_L\gamma^\mu b_L + \delta\kappa_R\bar{t}_R\gamma^\mu b_R\Big]W_\mu^+ + \text{h. c.} \\ &\quad -\frac{g}{2\cos\theta_W}\Big[(L_t+\delta L_t)\bar{t}_L\gamma^\mu t_L + (R_t+\delta R_t)\bar{t}_R\gamma^\mu t_R\Big]Z_\mu. \end{aligned}\tag{29}$$

For simplicity,[†] let us consider the case of anomalous $W^\pm$ couplings as shown in the diagram

[†]The anomalous Z-boson couplings are obtained in a similar manner, but there is the additional compli-

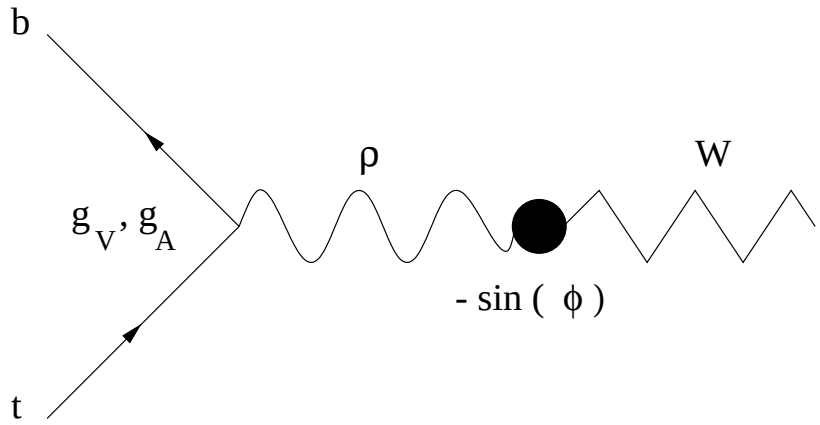

Figure 1: $W - V$ Mixing induced anomalous tbW coupling.

in Fig. 1. We find in the limit of large vector resonance mass that

$$\delta\kappa_L = -\frac{2}{\tilde{g}}(g_V - g_A), \quad \delta\kappa_R = -\frac{2}{\tilde{g}}(g_V + g_A). \tag{30}$$

There are several constraints on these couplings. The measurement of the rate for $b \to s\gamma$ restricts $|\delta\kappa_R| \lesssim 0.004$ [28, 29] but does not place significant constraints on $\delta\kappa_L$. An analysis of precision measurements at LEP [30] (with updated data from Ref. [31]) results in $|\delta\kappa_L| \lesssim 0.1$ *excluding* the parameter T.[‡] From future experiments, it is expected that a B factory can place significant further constraints of order $|\delta\kappa_R| \lesssim 0.001$, $|\delta\kappa_L| \lesssim 0.03$ [32]; and that single top production can yield $|\delta\kappa_L| \lesssim 0.05$ [33]. From all these numbers we conclude that a right-handed coupling is severely constrained and for the rest of this paper will concentrate on left-handed couplings exclusively. That is, we choose to satisfy the relation

$$g_A = -g_V, \tag{31}$$

and, in keeping with the current bounds, we will concentrate on the case

$$g_V \lesssim 0.03\ \tilde{g}. \tag{32}$$

cation of both ρ^0 and Z mixing with the photon.

[‡]If the parameter T is included, the bound could be stronger in certain cases. In our case, however, the induced anomalous couplings are of the form $\delta\kappa_L = \delta L_t$, and are not restricted by T where they appear in the combination $\delta\kappa_L - \delta L_t$ [30].

After these bounds are imposed, partial wave unitarity does not place additional constraints.

When new direct couplings such as those in Eq. (28) are introduced in a gauge invariant manner, as is done in the BESS model [27] (through their parameter b), the effective couplings $g_{V,A}$ of Eq. (28) receive contributions from both the direct couplings and mixing. In this general case Eq. (28) is not literally correct, as the charged and neutral couplings differ. We shall employ Eq. (28) for simplicity, assuming that the direct couplings dominate. For example, in the heavy vector limit of the BESS model, they take the form

$$g_V = -g_A = \frac{\tilde{g}}{4}\frac{b}{1+b}. \tag{33}$$

Considering both the charged and neutral vectors, this results in

$$\delta\kappa_L = \delta L_t = -\frac{1}{2}\frac{b}{1+b} \quad \text{and} \quad \delta\kappa_R = \delta R_t = 0. \tag{34}$$

The bound $|\delta\kappa_L| \lesssim 0.1$ then corresponds to $|b| \lesssim 0.25$. In this respect, it is expected that a future linear collider studying the reaction $e^+e^- \to W^+W^-$ can probe values of b some ten times smaller than this [34]. Our present study is complementary in the sense that we wish to observe the direct signal for a vector state production at high energies.

The couplings $g_{V,A}$ can be traded in favor of the physical partial decay widths via the relations

$$\Gamma_{\rho t\bar{t}} = \frac{M_\rho}{4\pi}\left(1-4\frac{m_t^2}{M_\rho^2}\right)^{\frac{1}{2}}\left\{{g_V}^2\left(1+2\frac{m_t^2}{M_\rho^2}\right)+{g_A}^2\left(1+4\frac{m_t^2}{M_\rho^2}\right)\right\} \tag{35}$$

$$\Gamma_{\rho t\bar{b}} = \frac{M_\rho}{4\pi}({g_V}^2+{g_A}^2)\left(1-\frac{m_t^2}{M_\rho^2}\right)^2\left(2+\frac{m_t^2}{M_\rho^2}\right) \tag{36}$$

$\Gamma_{\rho b\bar{b}}$ is the same as Eq. (35) replacing m_t by m_b. In our calculations, we consistently take $M_W = m_b = 0$.

In combining the ρ couplings to W_L in Eq. (24) with the couplings in Eq. (28), we obtain the scattering amplitudes

$$\begin{aligned}
\mathcal{M}_\rho^{++}(w^+w^- \to t\bar{t}) &= -\mathcal{M}_\rho^{--}(w^+w^- \to t\bar{t}) \\
&= a\tilde{g}g_V \frac{m_t\sqrt{s}}{s - M_\rho^2 + iM_\rho\Gamma_\rho} \cos\theta \\
\mathcal{M}_\rho^{\pm\mp}(w^+w^- \to t\bar{t}) &= \frac{a\tilde{g}}{2}\frac{s\sin\theta}{s - M_\rho^2 + iM_\rho\Gamma_\rho}(-g_V \mp g_A\beta_t)
\end{aligned} \tag{37}$$

and

$$\begin{aligned}
\mathcal{M}_\rho^{\pm\pm}(w^+z \to t\bar{b}) &= \frac{a\tilde{g}}{\sqrt{2}}\frac{m_t\sqrt{s}}{s - M_\rho^2 + iM_\rho\Gamma_\rho}\,\beta_m \\
&\quad \times\{(\mp g_V + g_A)(1+\cos\theta) + (\pm g_V - g_A)\} \\
\mathcal{M}_\rho^{\pm\mp}(w^+z \to t\bar{b}) &= \frac{a\tilde{g}}{\sqrt{2}}\frac{s}{s - M_\rho^2 + iM_\rho\Gamma_\rho}\beta_m(g_V \pm g_A)\sin\theta.
\end{aligned} \tag{38}$$

Unlike the case of the scalar resonance, these amplitudes do not grow with energy. For this reason, partial wave unitarity does not place any significant constraints. Also, unlike the case of a scalar resonance, the heavy vector resonance is narrow and a simple treatment of the constant width as above is adequate.

3 Sensitivity to the Top-SEWS Signal at Future Lepton Colliders

3.1 Effective W Approximation

The effective W-boson approximation (EWA) provides a viable simplification for high energy processes involving W-boson scattering [7]. It is particularly suitable for the calculations

under consideration since the W-boson level evaluation for the SEWS signal at high energies is adequate. The condition for the EWA to be valid is that the invariant energy scales are all much larger than the W mass, namely $s, |t|, |u| \gg M_W$. Besides, it is more accurate for a longitudinal W-boson due to the fact that the distribution function is largely independent of the W beam energies. To justify the EWA in our calculation, we compare our signal evaluation for a heavy scalar resonance with a full tree-level SM calculation [35]. We define the SM signal for a heavy Higgs boson σ_S following the subtraction procedure [22]

$$\sigma_S(M_H) = \sigma(M_H) - \sigma(M_H = 100 \ \text{GeV}). \tag{39}$$

The interpretation of this procedure is that the signal from a heavy Higgs boson should be defined as the enhancement over the perturbative SM expectation with a light ($M_H \sim 100$ GeV) Higgs boson, which should be viewed as the irreducible SM background.

The process of $e^+e^- \to Zt\bar{t}$ followed by $Z \to \nu\bar{\nu}$ leads to the same final state as our signal. It arises from different physics and needs to be removed from our consideration. We follow the earlier studies [36] to introduce a recoil mass against the observable $t\bar{t}$ system defined as

$$M^2_{rec} = s + m^2_{t\bar{t}} - 2\sqrt{s}(E_t + E_{\bar{t}}), \tag{40}$$

where E_t ($E_{\bar{t}}$) is the top (anti-top) quark energy in the e^+e^- CM frame. The recoil-mass spectrum peaks at M_Z for the background. Here and henceforth, we will impose $M_{rec} > 200\,\text{GeV}$ to effectively remove the $Z \to \nu\bar{\nu}$ background. We will adopt the same cut for the $e\nu\ tb$ process as well.

In Fig. 2, we present the production cross section for $e^+e^- \to \bar{\nu}\nu W^+W^- \to \bar{\nu}\nu t\bar{t}$ versus an invariant mass cut ($m^{cut}_{t\bar{t}}$) on the top quark pair for $M_H \to \infty$ at (a) e^+e^- CM energy $\sqrt{s} = 1.5$ TeV and (b) $\sqrt{s} = 4$ TeV. The solid curves are from the full SM calculation based on the subtraction scheme Eq. (39). The dotted curves are the Low Energy Theorem

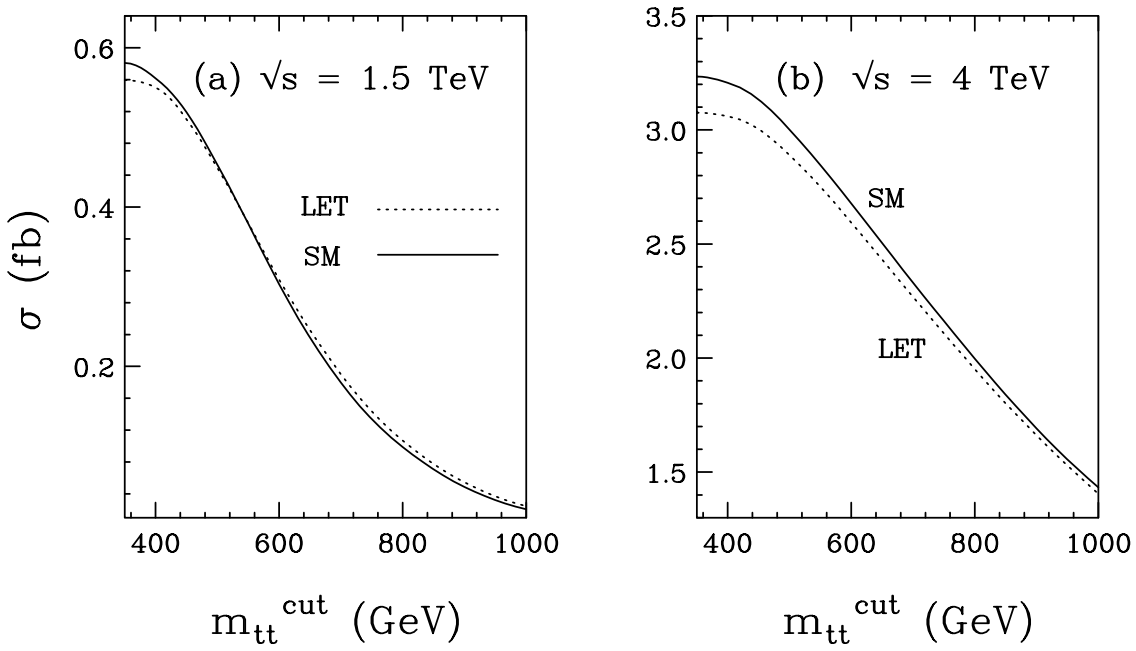

Figure 2: Production cross sections (in fb) for $e^+e^- \to \bar{\nu}\nu W^+W^- \to \bar{\nu}\nu t\bar{t}$ versus the invariant mass cut on the top quark pair for $M_H \to \infty$ at (a) $\sqrt{s} = 1.5\,\text{TeV}$ and (b) $\sqrt{s} = 4\,\text{TeV}$.

(LET) result for $w^+w^- \to t\bar{t}$ by EWA. The two calculations agree very well, especially for higher $m_{t\bar{t}}$ values.

In Fig. 3, we show the cross section for the same process, but versus the scattering angle cut ($\cos\theta_t^{cut}$) on the final state top quarks. In Fig. 3(a), we compare the scalar resonance model in Sec. 2.2 for $M_S = 1$ TeV (dashed curve) with the SM for $M_H = 1$ TeV (solid curve) based on the subtraction scheme Eq. (39). In both cases and henceforth, to preserve unitarity near the heavy scalar resonance, we adopt the prescription given in Eq. (13).

Fig. 3(b) compares the case for LET and the full SM calculation for $M_H \to \infty$. We see that the two calculations agree better for central scattering at low $\cos\theta_t$. These two figures motivate us to introduce the "basic acceptance cuts",

$$m_{t\bar{t}} > 500 \ \text{GeV}, \quad |\cos\theta_t| < 0.8. \tag{41}$$

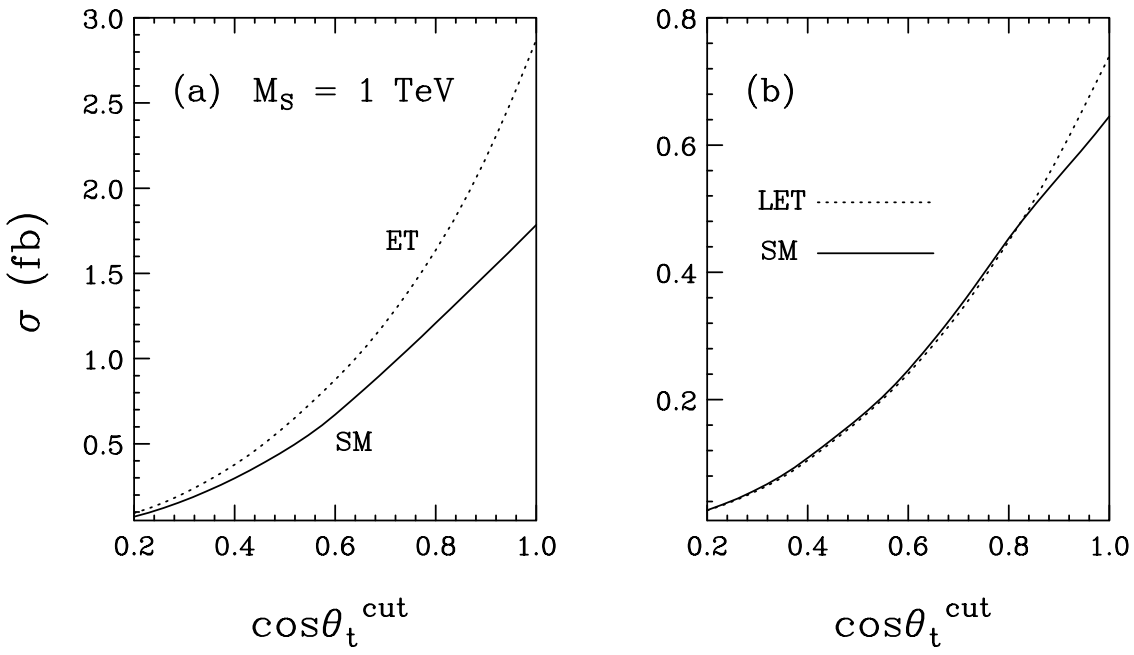

Figure 3: Production cross sections (in fb) for $e^+e^- \to \bar{\nu}\nu W^+W^- \to \bar{\nu}\nu\bar{t}t$ at $\sqrt{s} = 1.5$ TeV versus the polar angle cut on the final state t and $\bar{t}$ (a) for $M_S = 1$ TeV and (b) for $M_H \to \infty$.

These cuts not only guarantee the good agreement between the full SM calculation and the EWA that we will adopt for signal calculations beyond the SM, but are also necessary to enhance the signal over the SM backgrounds as we will discuss later. We impose a similar requirement for the tb process.

Finally we show the comparison of the two calculations versus the center of mass (CM) energy in Fig. 4 for (a) a 1 TeV scalar resonance and (b) $M_H \to \infty$, where the basic cuts of Eq. (41) have been imposed on both t and $\bar{t}$. The agreement is generally at order of 50% or better for $M_S = 1$ TeV and almost perfect for $M_H \to \infty$. We consider this to have justified our future use of the EWA in the signal calculations beyond the SM. However, we note that the EWA calculations for signal processes (1) and (2) do not properly incorporate the full kinematics of processes (3) and (4). We thus simulate the full kinematics and determine the cut efficiencies using the complete SM calculations in the next section.

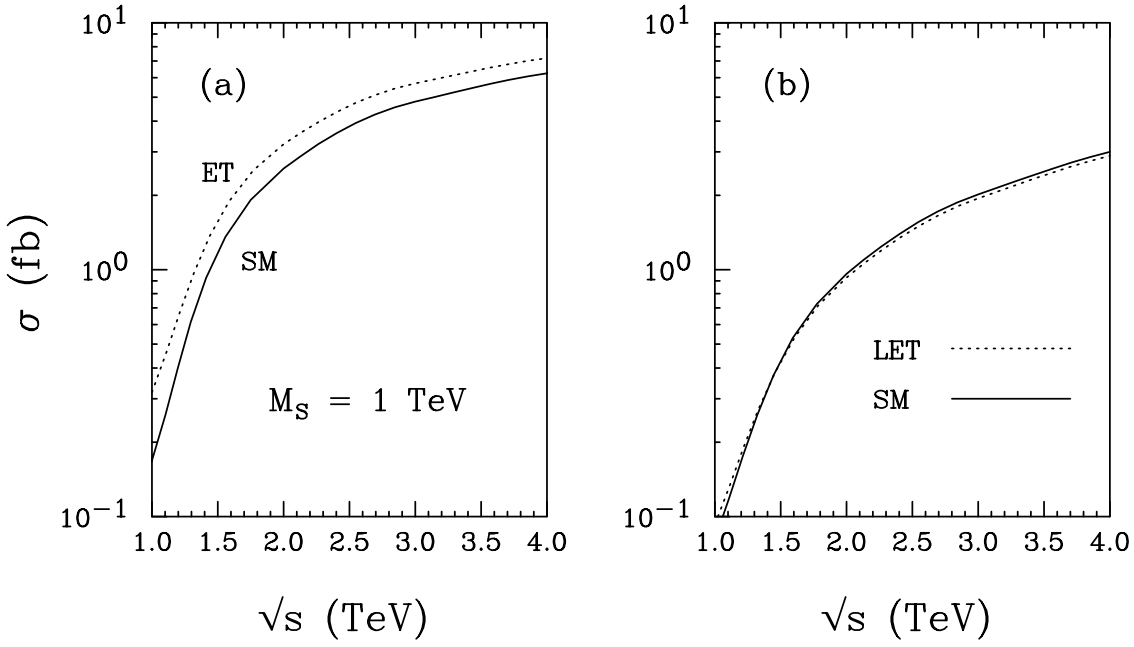

Figure 4: Production cross sections (in fb) for $e^+e^- \to \bar{\nu}\nu W^+W^- \to \bar{\nu}\nu\bar{t}t$ versus the CM energy for (a) $M_S = 1$ TeV and (b) $M_H \to \infty$.

3.2 Top-SEWS Signal and SM Backgrounds

For the SM-like heavy Higgs model adopted in the last section, the Higgs boson mass M_H is the only parameter. We would like to explore more general classes of strongly interacting electroweak models (SEWS) as outlined in Sec. 2. For a generic scalar singlet model, there are three input parameters: M_S, g_S, and κ as described in section 2.2. The two couplings can be traded by the physical partial widths and they are subject to the unitarity constraints Eqs. (15, 21, 23). In terms of the partial widths for $M_S = 1$ TeV, these constraints lead to

$$\begin{aligned} 80 \text{ GeV} \lesssim \quad \Gamma_{Sww} \quad &\lesssim 600 \text{ GeV}, \\ \Gamma_{Sww}\Gamma_{St\bar{t}} \quad &\lesssim (300 \text{ GeV})^2, \\ \Gamma_{St\bar{t}} \quad &\lesssim 420 \text{ GeV}, \end{aligned} \tag{42}$$

where we required that partial wave unitarity be satisfied up to $\sqrt{s_{ww}} = 2$ TeV.

The three input parameters for the vector model are $g_V(=-g_A)$, $\tilde{g}$, and a. These can be traded by the physical parameters M_ρ, $\Gamma_{\rho ww}$ (or $\Gamma_{\rho wz}$), and $\Gamma_{\rho t\bar{t}}$ (or $\Gamma_{\rho t\bar{b}}$). From the constraint of Eq. (32), we get for a neutral ρ^0 with mass $M_\rho = 1$ TeV,

$$\Gamma_{\rho t\bar{t}}\Gamma_{\rho ww} \lesssim (8 \text{ GeV})^2 \tag{43}$$

and for a charged $\rho^\pm$ of the same mass,

$$\Gamma_{\rho tb}\Gamma_{\rho wz} \lesssim (11 \text{ GeV})^2. \tag{44}$$

For the $W_L W_L \to t\bar{t}$ signal, the SM backgrounds are

$$e^+e^- \to e^+e^- t\bar{t}, \tag{45}$$

$$e^+e^- \to \bar{\nu}\nu W^+W^- \to \bar{\nu}\nu t\bar{t}. \tag{46}$$

Process (45) mainly comes from $\gamma\gamma \to t\bar{t}$ and has a large cross section, typically about 7.5 fb at $\sqrt{s} = 1.5$ TeV. The charged-current process Eq. (46) occurs at a lower rate, about 1.7 fb at $\sqrt{s} = 1.5$ TeV, but it is kinematically more difficult to separate from the signal. Following earlier studies [36, 37], we demand a high transverse momentum for the final state t and $\bar{t}$

$$p_T(t) > 150 \text{ GeV}, \tag{47}$$

which is motivated by the Jacobian peak in the p_T spectrum from a heavy particle decay. We also require a moderate momentum for the $t\bar{t}$ pair

$$30 \text{ GeV} < p_T(t\bar{t}) < 300 \text{ GeV}. \tag{48}$$

This cut forces the final state leptons to be away from the forward-backward collinear region. Since there are no energetic electrons in the central region for the signal process, we then veto events with final state electrons at large angle:

$$E_e > 50 \text{ GeV}, \quad |\cos\theta_e| < \cos(0.15 \text{ rad}). \tag{49}$$

We find that these cuts, along with the basic cuts (41), are very effective to suppress the SM backgrounds. The background (45) is largely eliminated by the combination of $p_T(t\bar{t})$ cut and electron veto. The effects of the cut on the charged current $t\bar{t}$ process are summarized in Table 1, again using the SM-like heavy Higgs model as the representative for the signal. From this table, we find the cut efficiencies of Eqs. (47,48,49) for the signal based on the subtraction scheme (39). They are

$$\epsilon = 83\% \quad \text{for} \quad \sqrt{s} = 1.5 \ \text{TeV}; \qquad \epsilon = 84\% \quad \text{for} \quad \sqrt{s} = 4 \ \text{TeV}. \tag{50}$$

For the remainder of this paper we use these cut efficiency figures for all the signal calculations within the EWA in the $W_L W_L \to t\bar{t}$ channel.

$\sqrt{s} = 1.5\,\text{TeV}$	$M_H = 1\,\text{TeV}$	Background $M_H = 0.1\,\text{TeV}$
cuts (41)	1.41 fb	0.21 fb
cuts (41,47,48,49)	1.13 fb	0.14 fb
$\sqrt{s} = 4\,\text{TeV}$	$M_H = 1\,\text{TeV}$	Background $M_H = 0.1\,\text{TeV}$
cuts (41)	8.86 fb	0.98 fb
cuts (41,47,48,49)	7.20 fb	0.55 fb

Table 1: Cross sections of process (46) for a SM-like heavy Higgs (1 TeV) and a light Higgs (0.1 TeV) with different cuts. This gives the cut efficiencies for Top-SEWS signals as in Eq. (50).

For the process $W_L Z_L \to tb$, the irreducible background is from

$$e^+e^- \to e\nu \ WZ \to e\nu \ tb. \tag{51}$$

Again, the largest contribution comes from the photon induced process $e\gamma \to \nu \ t\bar{b}$, where the other electron goes along the beam direction after emitting a collinear photon. For this

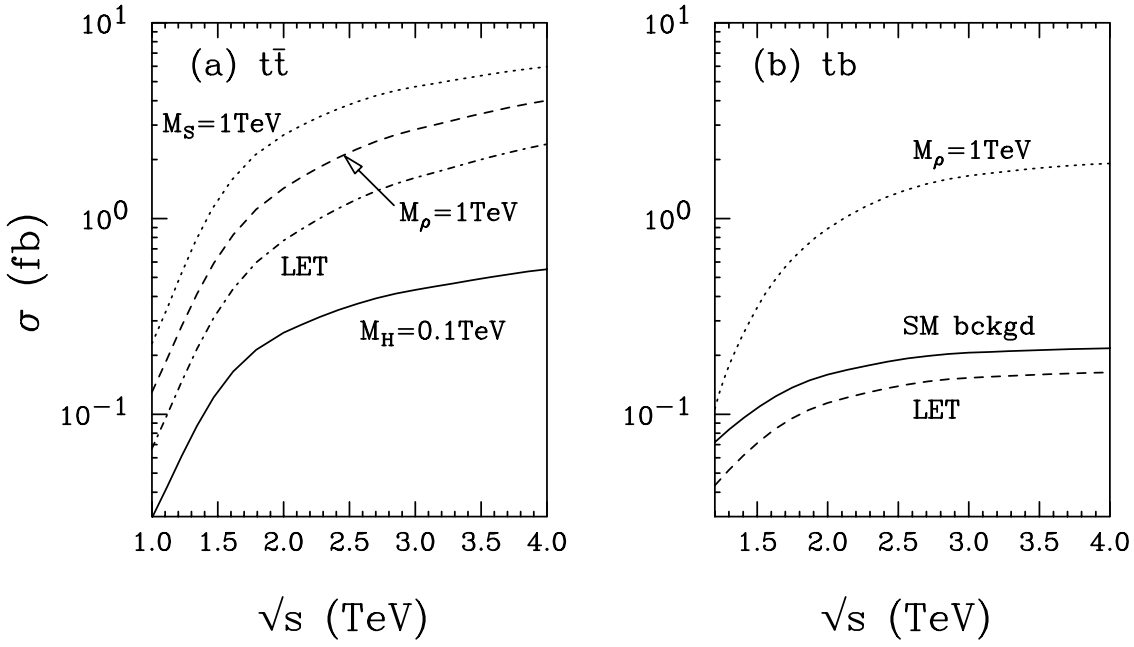

Figure 5: Production cross sections (in fb) for (a) $e^+e^- \to \bar{\nu}\nu W^+W^- \to \bar{\nu}\nu t\bar{t}$ versus $\sqrt{s}$ for $M_H = 0.1$ TeV (solid), LET (dot-dash), scalar singlet model (dots), and vector model (dashes), and for (b) $e^+e^- \to e\nu\ WZ \to e\nu\ tb$ versus $\sqrt{s}$ for the vector model (dots), LET (dashes) and SM background (solid) with the full cuts imposed. We have used the model parameters as in Eqs. (55) and (56).

case, we impose the cuts (41) and (47). Since there is a final state electron in the signal process with a typical transverse momentum of $M_Z/2$, we require an electron tagging at a finite angle

$$|\cos\theta_e| < \cos(0.15 \text{ rad}). \tag{52}$$

This electron tagging is very effective to remove the SM background, and more so at higher energies. The combination of the above cuts significantly reduces the $e\gamma$ process and brings the background to a level below the signal rate.

To determine the signal efficiency of the electron tagging, we calculate the process

$$e^+e^- \to \bar{\nu}e^-\rho^+. \tag{53}$$

We find

$$\epsilon = 93\% \quad \text{for} \quad \sqrt{s} = 1.5 \ \text{TeV}; \qquad \epsilon = 61\% \quad \text{for} \quad \sqrt{s} = 4 \ \text{TeV}, \tag{54}$$

which will be used for other signal calculations in the $W_L W_L \to tb$ channel based on the EWA. The lower tagging efficiency at 4 TeV is due to the fact that the final state electron becomes more forward at higher energies.

We now present the production cross sections for the signal and background versus the CM energy $\sqrt{s}$ after the cuts. Fig. 5(a) is for $e^+e^- \to \bar{\nu}\nu W^+W^- \to \bar{\nu}\nu \ \bar{t}t$ process with the full cuts (41, 47, 48, 49) for the scalar model (dots), vector model (dashes), LET (dot-dash), and the irreducible background $M_H = 0.1$ TeV (solid). For illustration, we have taken the model parameters to be

$$\begin{aligned} M_S = 1 \ \text{TeV}, \ \Gamma_{Sww} = 493 \ \text{GeV}, \ \Gamma_{St\bar{t}} = 50 \ \text{GeV}, \\ M_\rho = 1 \ \text{TeV}, \ \Gamma_{\rho ww} = 50 \ \text{GeV}, \ \Gamma_{\rho t\bar{t}} = 1.3 \ \text{GeV}. \end{aligned} \tag{55}$$

Figure 5(b) shows the production cross sections for $e^+e^- \to e\nu \ WZ \to e\nu \ tb$, with the cuts (41, 47, 52) for the vector model (dots), LET (dashes), and the SM background (solid). The model parameters are taken as

$$M_\rho = 1 \ \text{TeV}, \ \Gamma_{\rho ww} = 50 \ \text{GeV}, \ \Gamma_{\rho tb} = 2.5 \ \text{GeV}. \tag{56}$$

We see from Fig. 5 that our cuts effectively suppress the SM background below the signal for both channels. The signal rate at a 1.5 TeV linear collider is typically between 0.5 and 1.2 fb.

3.3 Results and discussion

For the remainder of our analysis, we consider the top quark to decay hadronically $t \to bW \to bjj'$ with a branching fraction approximately 70%. In doing so, we assume that we

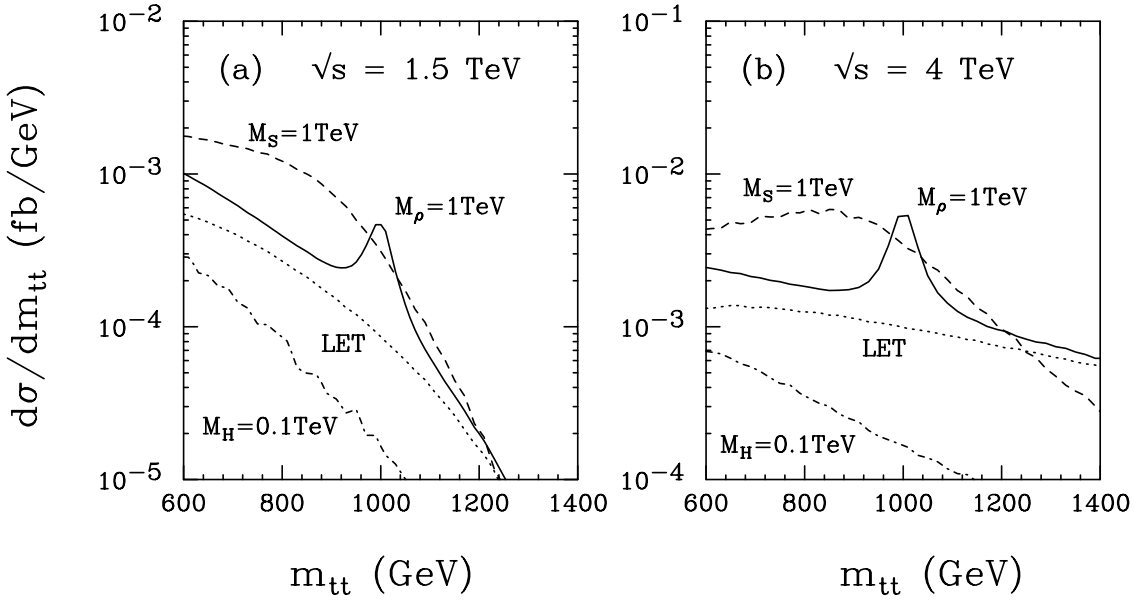

Figure 6: Signal and background differential cross sections versus $t\bar{t}$ invariant mass for (a) $\sqrt{s} = 1.5$ TeV and (b) $\sqrt{s} = 4$ TeV: SM background by $M_H = 0.1$ TeV (dot-dash), LET (dots), scalar model (dashes), and vector model (solid). We have used the model parameters as in Eq. (55). All cuts are imposed and the branching fraction for $t \to bjj'$ is included.

can fully reconstruct the t and $\bar{t}$ events, and that there are no isolated central electrons from the decay to confuse our electron vetoing and tagging requirements. We also assume a data sample of 200 fb^{-1} at $\sqrt{s} = 1.5$ TeV. We can see from Fig. 5 that we may reach a clear signal observation for both a scalar and a vector resonance in the $t\bar{t}$ channel. Although the LET channel has relatively lower rate, it may nevertheless lead to about 35 events after including the branching fraction, which is well above the background expectation. For the tb channel, both signal and background rates are slightly smaller than the $t\bar{t}$ case, but the vector signal rate is still sufficiently above background to be observable. The LET amplitude in this case is below background as was already seen in the model discussions.

It is important to know how well one can reconstruct the signal and contrast it with the background beyond simple event counting. In Fig. 6 we show the distributions for the signal and background versus $t\bar{t}$ invariant mass ($m_{t\bar{t}}$) for (a) $\sqrt{s} = 1.5$ TeV and (b)

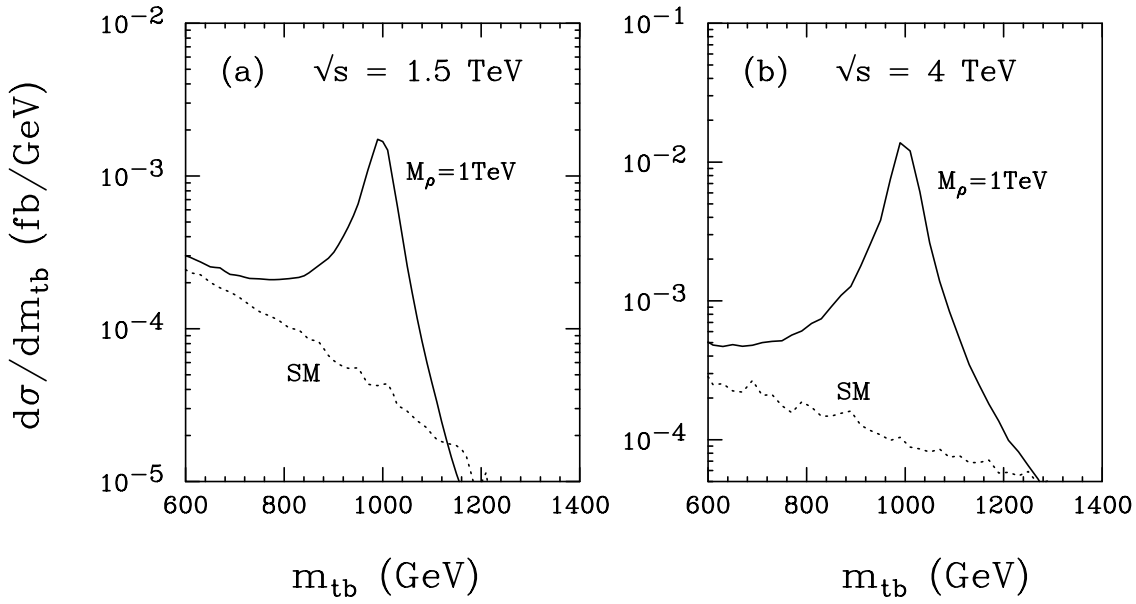

Figure 7: Signal and background cross sections (in fb) versus tb invariant mass (m_{tb}) for (a) $\sqrt{s} = 1.5$ TeV and (b) $\sqrt{s} = 4$ TeV: SM (dots) and vector model (solid). We have used the model parameters as in Eq. (56). All cuts are imposed and the branching fraction for $t \to bjj'$ is included.

$\sqrt{s} = 4$ TeV with the SM background represented by $M_H = 0.1$ TeV (dot-dash), LET signal (dots), scalar model (dashes), and vector model (solid). The model parameters are taken as in Eq. (55). All cuts are imposed and the branching fraction for $t\bar{t}$ decay is included. We see a broad resonance around $M_S = 1$ TeV in scalar model due to its large width. For the vector case, however, the width is narrower in general and the signal peaks above the scalar model for $M_\rho = 1$ TeV in a distinctive manner. The LET model has relatively low rate and has no particular structure. In Fig. 7 we show the same signal and background distributions, but for the tb channel versus the invariant mass (m_{tb}). The model parameters are taken as in Eq. (56). Clearly, the observation of a signal in Fig. 7 would provide decisive information to discriminate a scalar resonance from a vector. The authors of Ref. [15] use, instead, the top-quark polarization information to distinguish a scalar from a vector resonance.

We next consider the extent to which one can probe the couplings for different models.

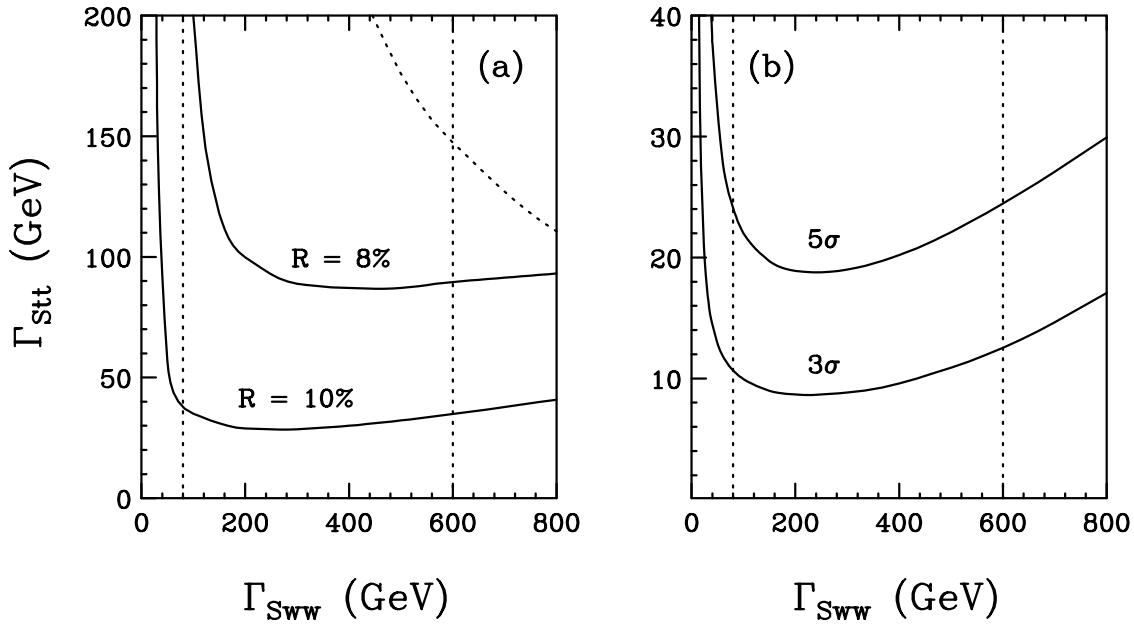

Figure 8: At a linear collider with $\sqrt{s} = 1.5$ TeV and a luminosity of 200 fb^{-1}, (a) accuracy contours of determination of the partial widths for the scalar resonance model with $M_S = 1$ TeV; (b) statistical significance contours to distinguish a 1 TeV scalar from LET. Dotted lines are unitarity constraints given in Eq. (42).

Fig. 8(a) shows the accuracy contours to determine the partial decay widths (thus the couplings) in the scalar resonance model with $M_S = 1$ TeV at $\sqrt{s} = 1.5$ TeV and a luminosity of 200 fb^{-1}. The statistical accuracy for the cross section measurement is defined as

$$R \;=\; \frac{\sqrt{S+B}}{S}$$

where S and B are the number of signal and background events respectively and we have ignored the experimental systematic effects. We find that partial widths can be probed up to about 10% accuracy for $\Gamma_{St\bar{t}} \approx 50$ GeV within the unitarity bounds shown as dotted lines (Eq. 42). In the region above the curve labeled $R = 8\%$, the partial widths can be determined to 8% or better accuracy.

Also shown in Fig. 8(b) are the statistical significance contours to distinguish a 1 TeV

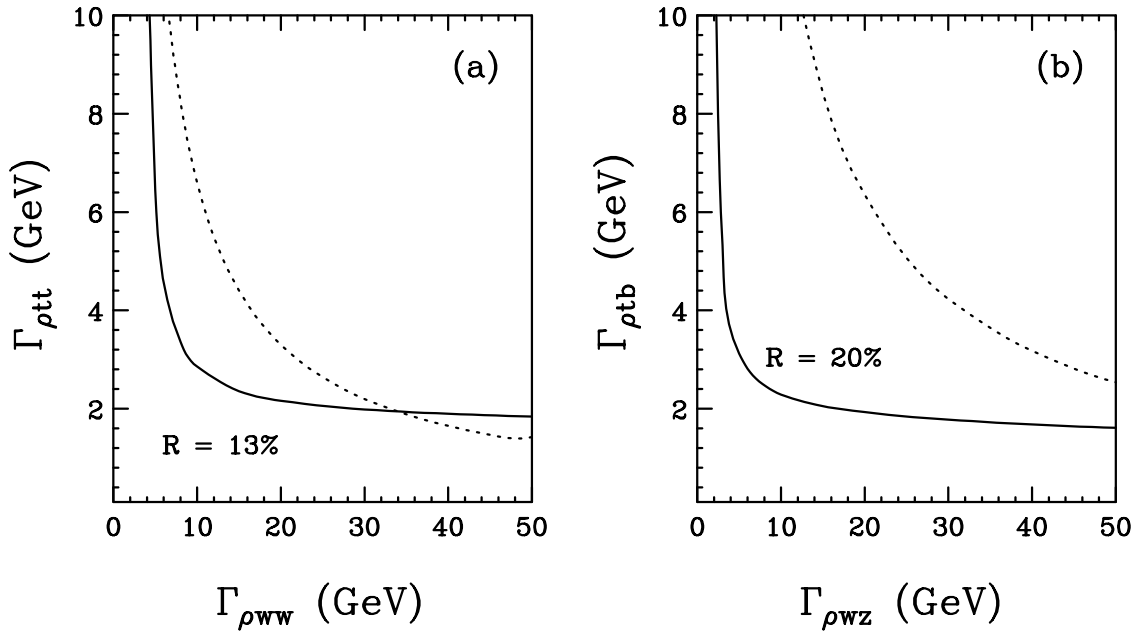

Figure 9: At a linear collider with $\sqrt{s} = 1.5$ TeV and a luminosity of 200 fb^{-1}, determination of the partial widths for the vector resonance model with $M_\rho = 1$ TeV (a) 13% accuracy contour for $W^+W^- \to \rho^0 \to t\bar{t}$ channel; (b) 20% accuracy contour for $W^\pm Z \to \rho^\pm \to t\bar{b}(\bar{t}b)$. Dotted lines are from the current low energy constraints in Eqs. (43) and (44).

scalar signal from the LET amplitudes. Here we define an appropriate standard deviation as

$$\sigma \;=\; \frac{\{\sigma(\Gamma_{St\bar{t}}, \Gamma_{Sww}) - \sigma(0,0)\}\mathcal{L}}{\sqrt{\sigma(0,0)\mathcal{L}}}$$

where $\sigma(\Gamma_{St\bar{t}}, \Gamma_{Sww})$ is the cross section in the scalar model for the given widths, $\sigma(0,0)$ is the non-resonance cross section with $g_S = \kappa = 0$, and $\mathcal{L}$ is the luminosity. It is easy to see that the scalar model is distinguishable at the 5σ level from the non-resonant case within the unitarity limits given in Eq. (42).

We show the same analysis for the vector model in Fig. 9, where we present the sensitivity to the vector resonance model with $M_\rho = 1$ TeV at $\sqrt{s} = 1.5$ TeV and a luminosity of 200 fb^{-1}, for (a) 13% accuracy determination of the partial widths for $W^+W^- \to \rho^0 \to t\bar{t}$

and (b) 20% accuracy determination of the partial widths for $W^{\pm}Z \to \rho^{\pm} \to t\bar{b}$ ($\bar{t}b$). We found in Fig. 9(a) that a 13% accuracy determination of the partial widths is possible for the neutral vector process in the region allowed by the current bounds given in Eq. (43). For the charged process we have a smaller signal rate, nevertheless, we found in Fig. 9(b) that we can still determine the partial widths to 20% accuracy in the region allowed by current constraints, Eq. (44).

4 Conclusion

We have studied the couplings of the top quark to TeV resonances that occur in models in which the electroweak symmetry is broken by a strong interaction. Our study is motivated by the fact that in many models the top quark plays a special role in the breaking of electroweak symmetry.

We have explored the possibility that the new physics is realized as a scalar resonance or a vector resonance near 1 TeV, as well as the case where the resonance is beyond reach (LET). For the scalar model, we used partial wave unitarity to constrain the parameters as shown in Sec. 2.2. For the vector model, we used current experimental data to constrain the parameter space as presented in Sec. 2.3. We found within these constraints, that signal rates in these models at future lepton colliders can be well above the SM backgrounds after judicial cuts are applied. The models can be distinguished from each other by systematically studying two different final states. Typically one would see a broad scalar resonance S, or a relatively narrow vector resonance ρ^0 in the $t\bar{t}$ channel and a narrow vector resonance $\rho^{\pm}$ in the tb channel. In particular, we illustrated our results at a 1.5 TeV linear collider with an integrated luminosity of 200 fb^{-1}. One expects to observe about 120 events for either $S \to t\bar{t}$ or $\rho^{0,\pm} \to t\bar{t},\ tb$ including final state identification. Even if the lower-lying resonances

are inaccessible at the collider, one can still observe a statistically significant deviation as predicted by the LET for the $t\bar{t}$ final state from the perturbative SM expectation. Finally, the leading partial decay widths, which characterize the coupling strengths, can be statistically determined to about 10% level.

Acknowledgments: The work of T.H. and Y.J.K. was supported in part by the US DOE under contract No. DE-FG02-95ER40896 and in part by the Wisconsin Alumni Research Foundation. The work of A.L. was supported in part by the RFBR grants 99-02-16558 and 00-15-96645. The work of G.V. was supported in part by DOE under contact number DE-FG02-92ER40730. G.V. thanks the Special Research Centre for the Subatomic Structure of Matter at the University of Adelaide for their hospitality and partial support while part of this work was completed.

Appendix A SM amplitudes using the Equivalence Theorem

In this appendix, we present the standard model amplitudes obtained using the Equivalence Theorem for the processes $w^-w^+ \to t\bar{t}$, $zz \to t\bar{t}$, and $zw^+ \to t\bar{b}$. From these amplitudes one can derive the (LET) amplitudes by taking the large Higgs mass limit, ignoring the electroweak couplings, and setting $m_b = 0$.

$\underline{w^-w^+ \to t\bar{t}}$

$$\begin{aligned}
\mathcal{M}^{\pm\pm}{}_H(ww \to t\bar{t}) &= \pm\frac{{M_H}^2}{(s-{M_H}^2)}\frac{m_t\sqrt{s}}{v^2}\beta_t \\
\mathcal{M}^{\pm\mp}{}_H(ww \to t\bar{t}) &= 0 \qquad \text{(A1)} \\
\mathcal{M}^{\pm\pm}{}_b(ww \to t\bar{t}) &= \mp\frac{2m_t^3}{v^2\sqrt{s}}\frac{\beta_t+\cos\theta}{1+\beta_t\cos\theta-2m_t^2/s} \\
\mathcal{M}^{\pm\mp}{}_b(ww \to t\bar{t}) &= \frac{m_t^2}{v^2}\frac{(1\pm\beta_t)\sin\theta}{1+\beta_t\cos\theta-2m_t^2/s} \qquad \text{(A2)} \\
\mathcal{M}^{\pm\pm}{}_\gamma(ww \to t\bar{t}) &= \pm 2g^2x_WQ\frac{m_t}{\sqrt{s}}\cos\theta \\
\mathcal{M}^{\pm\mp}{}_\gamma(ww \to t\bar{t}) &= \mp g^2x_WQ\sin\theta \qquad \text{(A3)} \\
\mathcal{M}^{\pm\pm}{}_Z(ww \to t\bar{t}) &= \pm 2g_Vg_Z^2(\frac{1}{2}-x_W)\frac{m_t}{\sqrt{s}}\cos\theta \\
\mathcal{M}^{\pm\mp}{}_Z(ww \to t\bar{t}) &= (-g_V\mp g_A\beta_t)g_Z^2(\frac{1}{2}-x_W)\sin\theta \qquad \text{(A4)}
\end{aligned}$$

where

$$\beta_t = (1-4m_t^2/s)^{\frac{1}{2}}, \quad x_W = \sin^2\theta_W, \quad g_Z = \frac{g}{\cos\theta_W}, \quad g_V = \frac{1}{2}T_3 - Qx_W, \quad \text{and} \quad g_A = -\frac{1}{2}T_3.$$

Taking the limit $M_H^2 \gg s$ and ignoring the terms of order g^2, we find to leading order,

$$\begin{aligned} \text{LET}: \quad \mathcal{M}^{\pm\pm}{}_{LET}(ww \to t\bar{t}) &= \mp\frac{m_t\sqrt{s}}{v^2}\beta_t \\ \mathcal{M}^{\pm\mp}{}_{LET}(ww \to t\bar{t}) &= \frac{m_t^2}{v^2}\frac{(1 \pm \beta_t)\sin\theta}{1 + \beta_t\cos\theta - 2m_t^2/s}. \end{aligned}$$

<u>$zz \to t\bar{t}$</u>

$$\begin{aligned} \mathcal{M}^{\pm\pm}{}_{H}(zz \to t\bar{t}) &= \pm\frac{{M_H}^2}{(s - {M_H}^2)}\frac{m_t\sqrt{s}}{v^2}\beta_t \\ \mathcal{M}^{\pm\mp}{}_{H}(zz \to t\bar{t}) &= 0 \qquad \text{(A5)} \\ \mathcal{M}^{\pm\mp}{}_{top}(zz \to t\bar{t}) &= \pm\frac{2m_t^3}{v^2\sqrt{s}}\frac{\beta_t + \cos\theta}{1 + \beta_t\cos\theta} \\ \mathcal{M}^{\pm\mp}{}_{top}(zz \to t\bar{t}) &= -\frac{m_t^2}{v^2}\frac{\sin\theta}{1 + \beta_t\cos\theta}. \qquad \text{(A6)} \end{aligned}$$

$$\begin{aligned} \text{LET}: \quad \mathcal{M}^{\pm\pm}{}_{LET}(zz \to t\bar{t}) &= \mp\frac{m_t\sqrt{s}}{v^2}\beta_t \\ \mathcal{M}^{\pm\mp}{}_{LET}(zz \to t\bar{t}) &= -\frac{m_t^2}{v^2}\frac{\sin\theta}{1 + \beta_t\cos\theta}. \qquad \text{(A7)} \end{aligned}$$

Again we keep only the leading order terms and ignore the top-quark exchange diagram for $\mathcal{M}^{\pm\pm}{}_{LET}(zz \to\ t\bar{t})$.

<u>$zw^+ \to t\bar{b}$</u>

$$\mathcal{M}^{++}{}_{W^+}(zw^+ \to t\bar{b}) = -\frac{\sqrt{2}}{4}g^2\frac{m_t}{\sqrt{s}}\beta_m\cos\theta$$

$$\begin{aligned}
\mathcal{M}^{--}{}_{W^+}(zw^+ \to t\bar{b}) &= \mathcal{M}^{+-}{}_{W^+}(zw^+ \to t\bar{b}) = 0 \\
\mathcal{M}^{-+}{}_{W^+}(zw^+ \to t\bar{b}) &= \frac{\sqrt{2}}{4} g^2 \beta_m \sin\theta
\end{aligned} \tag{A8}$$

where $\beta_m = (1 - m_t^2/s)^{1/2}$.

$$\begin{aligned}
\mathcal{M}^{++}{}_{top}(zw^+ \to t\bar{b}) &= \frac{\sqrt{2} m_t^3}{v^2 \sqrt{s}} \frac{\beta_m (1 + \cos\theta)}{[\beta_m^2 (1 - \cos\theta) + 2m_t^2/s]} \\
\mathcal{M}^{--}_{top}(zw^+ \to t\bar{b}) &= \mathcal{M}^{+-}_{top}(zw^+ \to t\bar{b}) = 0 \\
\mathcal{M}^{-+}{}_{top}(zw^+ \to t\bar{b}) &= -\frac{\sqrt{2} m_t^2}{v^2} \frac{\beta_m \sin\theta}{[\beta_m^2 (1 - \cos\theta) + 2m_t^2/s]}
\end{aligned} \tag{A9}$$

where $\mathcal{M}_b(zw^+ \to t\bar{b})$ is proportional to m_b and is neglected.

$$\begin{aligned}
\text{LET}: \quad \mathcal{M}^{++}{}_{LET}(zw^+ \to t\bar{b}) &= \frac{\sqrt{2} m_t^3}{v^2 \sqrt{s}} \frac{\beta_m (1 + \cos\theta)}{[\beta_m^2 (1 - \cos\theta) + 2m_t^2/s]} \\
\mathcal{M}^{-+}{}_{LET}(zw^+ \to t\bar{b}) &= -\frac{\sqrt{2} m_t^2}{v^2} \frac{\beta_m \sin\theta}{[\beta_m^2 (1 - \cos\theta) + 2m_t^2/s]}.
\end{aligned} \tag{A10}$$

References

[1] For a review, see *e. g.*, M. Chanowitz, Ann. Rev. Nucl. Part. Sci. **38**, 323 (1988).

[2] C. Hill, Phys. Lett. **B266**, 419 (1991); *ibid.* **B345**, 483 (1995); E. Eichten and K. Lane, Phys. Lett. **B352**, 382 (1995).

[3] B. Dobrescu and C. Hill, Phys. Rev. Lett. **81**, 2634 (1998); R. S. Chivukula, B. Dobrescu, H. Georgi, and C. Hill, Phys. Rev. **D59**, 075003 (1999); G. Burdman and N. Evans, Phys. Rev. **D59**, 115005 (1999).

[4] E. H. Simmons, hep-ph/9908488.

[5] B. W. Lee, C. Quigg, and H. B. Thacker, Phys. Rev. **D16**, 1519 (1977); M.S. Chanowitz and M.K. Gaillard, Nucl. Phys. **B261**, 379 (1985); Y.P. Yao and C.P. Yuan, Phys. Rev. **D38**, 2237 (1988); J. Bagger and C. Schmidt, Phys. Rev. **D41**, 264 (1990); H. Veltman, Phys. Rev. **D41**, 2294 (1990); H.-J. He, Y.-P. Kuang, and X. Li, Phys. Rev. Lett. **69**, 2619 (1992); H.-J. He and W.B. Kilgore, Phys. Rev. **D55**, 1515 (1997).

[6] M. Chanowitz, M. Furman and I. Hinchliffe, Nucl. Phys. **B153**, 402 (1979).

[7] M. Chanowitz and M.K. Gaillard, Phys. Lett. **B142**, 85 (1984); G. Kane, W. Repko and W. Rolick, Phys. Lett. **B148**, 367 (1984); S. Dawson, Nucl. Phys. **B249**, 42 (1985).

[8] R.P. Kauffman, Phys. Rev. **D41**, 3343 (1990).

[9] M. Gintner and S. Godfrey, in the Proceedings of *New Directions for High-Energy Physics*, June 25-July 12, 1996, Snowmass, p. 824.

[10] F. Larios, E. Malkawi and C.P. Yuan, Acta Phys. Polon. **B27**, 3741 (1996); F. Larios and C.-P. Yuan, Phys. Rev. **D55**, 7218 (1997); Jose Wudka, talk given at *the 5th*

International Conference on Physics Beyond the Standard Model, Balholm, Norway, 29 Apr - 4 May 1997, hep-ph/9706434.

[11] T. Barklow, in the Proceedings of *New Directions for High-Energy Physics*, June 25-July 12, 1996, Snowmass, p. 819; T. Han, hep-ph/9910495.

[12] F. Larios, Tim Tait, and C.-P. Yuan, Phys. Rev. **D57**, 3106 (1998).

[13] V. Barger, M. Berger, J. Gunion and T. Han, talk given at *ITP Conference on Future High-energy Colliders*, Santa Barbara, CA, 21-25 Oct 1996, hep-ph/9704290.

[14] T. Barklow *et al.*, in the Proceedings of *New Directions for High-Energy Physics*, June 25-July 12, 1996, Snowmass, p. 735.

[15] E. R. Morales and M. E. Peskin, hep-ph/9909383.

[16] M.S. Chanowitz, M. Golden and H. Georgi, Phys. Rev. Lett. **57**, 2344 (1986); Phys. Rev. **D35**, 1149 (1987).

[17] A. Dobado and M. Herrero, Phys. Lett. **B228**,495 (1989); *ibid.* **B233**, 505 (1989); J. Donoghue and C. Ramirez, Phys. Lett. **B234**, 361 (1990); S. Dawson and G. Valencia, Nucl. Phys. **B348**, 23 (1991); *ibid.* **B352**, 27 (1991).

[18] R. D. Peccei, S. Peris, and X. Zhang, Nucl. Phys. **B349**, 305 (1991).

[19] T. Appelquist and M. Chanowitz, Phys. Rev. Lett. **59**, 2405 (1987).

[20] W. Marciano, G. Valencia and S. Willenbrock, Phys. Rev. **D40**, 1725 (1989).

[21] J. Bagger, S. Dawson and G. Valencia, Nucl. Phys. **B399**, 364 (1993).

[22] J. Bagger, V. Barger, K. Cheung, J. Gunion, T. Han, G. Ladinsky, R. Rosenfeld, C.-P. Yuan, Phys. Rev. **D49**, 1246 (1994); *ibid.* **D52**, 3878 (1995).

[23] M.H. Seymour, Phys. Lett. **B354**, 409 (1995).

[24] G. Valencia and S. Willenbrock, Phys. Rev. **D42**, 853 (1990); *ibid.* **D46**, 2247 (1992).

[25] S. Jager and S. Willenbrock, Phys. Lett. **B435**, 139 (1998); R. S. Chivukula, Phys. Lett. **B439**, 389 (1998).

[26] J. Bagger, T. Han and R. Rosenfeld, FERMILAB-CONF-90-253-T, published in *Snowmass Summer Study 1990*, p. 208.

[27] R. Casalbuoni *et al.*, Phys. Lett. **B155**, 95 (1985); Nucl. Phys. **B282**, 235 (1987); *ibid.* **B310**, 181 (1988); Phys. Lett. **B249**, 130 (1990); *ibid.* **B253**, 275 (1991).

[28] K. Fujikawa and A. Yamada, Phys. Rev. **D49**, 5890 (1994).

[29] F. Larios, M. A. Perez and C. P. Yuan, Phys. Lett. **B457**, 334 (1999).

[30] S. Dawson and G. Valencia, Phys. Rev. **D53**, 1721 (1996).

[31] C. Caso *et al.*, Eur. Phys. J. **C3**, 1 (1998).

[32] A. A. El-Hady and G. Valencia, Phys. Lett. **B414**, 173 (1997).

[33] T. Tait and C. P. Yuan, hep-ph/9710372.

[34] D. Dominici, Riv. Nuovo Cim. **20**, 1 (1997) [hep-ph/9711385].

[35] For the full SM calculations, we have made use of the Madgraph package by T. Stelzer and W.F. Long, Comput. Phys. Commun. **81**, 357 (1994).

[36] V. Barger, K. Cheung, T. Han and R.J.N. Phillips, Phys. Rev. **D52**, 3815 (1995); V. Barger, M. Berger, J. Gunion and T. Han, Phys. Rev. **D55**, 142 (1997).

[37] V. Barger, K. Cheung, T. Han and R.J.N. Phillips, Phys. Rev. **D42**, 3052 (1990).